Critical Chemical Equivalence(CCE): The SymC Principle Governing Catalysis and Reactivity

Nate Christensen

Independent Researcher
SymC Universe Project, Missouri, USA
NateChristensen@SymCUniverse.com

10 December 2025

Abstract

The ratio $\chi = \Gamma/(2\Omega)$—damping rate to characteristic frequency—organizes chemical reactivity across multiple domains. This paper demonstrates that (i) adiabatic versus nonadiabatic electron transfer corresponds to $\chi > 1$ versus $\chi < 1$, (ii) concerted versus stepwise proton-coupled electron transfer reflects whether χ remains within or oscillates through the critical window, and (iii) catalytic bond activation occurs when the catalyst tunes the substrate toward $\chi \approx 1$. This framework unifies Marcus theory, proton-coupled electron transfer mechanism selection, and the Sabatier principle under a single stability criterion derived from the Symmetrical Convergence (SymC) postulate. Illustrative comparisons with TEMPO self-exchange kinetics showing $k_{\text{et}} \propto 1/\tau_L$ across solvents, and N_2 dissociation on Fe surfaces where barrier reduction from 1.1 eV (Fe(110)) to 0.3 eV (Fe(111)) tracks χ moving toward unity, are consistent with the framework's predictions. The approach yields falsifiable predictions for solvent effects, isotope effects, and spectroscopic signatures across all three domains.

Definition of Critical Chemical Equivalence(CCE):
A chemical transformation achieves maximum efficiency when its dissipation rate (Γ) equals twice its characteristic frequency (2Ω), creating critical damping where eigenvalues coalesce and oscillatory return transforms into irreversible completion.

Keywords: Critical damping; Electron transfer; Marcus theory; Proton-coupled electron transfer; Catalysis; Stability ratio; Nitrogen fixation; Kramers turnover

1 Introduction: The Missing Variable

Chemical reactivity has traditionally been characterized through thermodynamic metrics: free energy changes ΔG, reorganization energies λ, binding energies, and activation barriers. These quan-

tities determine *whether* a reaction is favorable and provide estimates of *how fast* it proceeds. However, they do not address a more fundamental question: *what determines whether a chemical transformation completes or reverses?*

Consider three puzzles from disparate areas of chemistry:

1. **Electron transfer:** Marcus theory successfully predicts rate constants across many orders of magnitude, yet systems with similar thermodynamic parameters sometimes show dramatically different yields of charge-separated products. Some donor-acceptor pairs transfer electrons efficiently; others undergo rapid back-electron-transfer despite identical driving forces.

2. **Proton-coupled electron transfer:** Reactions involving simultaneous movement of electrons and protons can proceed through stepwise pathways (electron-first or proton-first) or through concerted mechanisms. The conditions determining which pathway dominates remain incompletely understood, with recent high-pressure experiments revealing mechanism switching under conditions that leave thermodynamic parameters largely unchanged.

3. **Catalytic bond activation:** The Haber-Bosch process for nitrogen fixation requires temperatures exceeding 400°C and pressures above 200 atm, yet biological nitrogenase enzymes achieve the same transformation at ambient conditions. Both systems break the same N≡N triple bond; the thermodynamics are identical. Something beyond energetics determines efficiency.

These puzzles share a common feature: while thermodynamic descriptions successfully predict equilibrium properties and rate constants, they do not fully capture the dynamical factors determining reaction completion versus reversal. The missing element is dynamical: χ **measures whether a reaction coordinate wiggles (oscillates back), sticks (relaxes slowly), or flows (completes irreversibly).**

This paper introduces a single dimensionless parameter that organizes all three phenomena:

$$\boxed{\chi \equiv \frac{\Gamma}{2\Omega}} \tag{1}$$

where Ω is the characteristic frequency of the relevant chemical coordinate and Γ is the damping rate (energy dissipation into the environment).

Unit convention: Throughout this paper, Γ and Ω denote rates (dimensions of inverse time: s^{-1}, rad/s). When spectroscopic linewidths ΔE (energy units: eV, cm^{-1}) or vibrational frequencies ν (frequency units: Hz, cm^{-1}) are used, conversions follow: $\Gamma_{\text{rate}} = \Delta E/\hbar$ (converting energy linewidth to rate) and $\Omega = 2\pi\nu$ (converting frequency to angular frequency). The energy-space expression $\chi = \Delta E/(2h\nu)$ is algebraically equivalent to the rate-space definition $\chi = \Gamma/(2\Omega)$; no new physics is introduced, only a change of units for experimental convenience.

The parameter χ is the dynamical stability ratio, a concept that emerges independently from multiple theoretical frameworks: Kramers' 1940 barrier-crossing theory, Zusman's solvent-controlled

electron transfer, and Grote-Hynes friction corrections to transition state theory all exhibit optimal behavior near $\chi \approx 1$. The Symmetrical Convergence (SymC) framework recognizes this convergent pattern as a universal organizing principle across adaptive systems. At $\chi = 1$, the system undergoes a fundamental transition: eigenvalues coalesce, oscillatory dynamics transform into monotonic relaxation, and the system achieves fastest energy dissipation without overshoot. This boundary separates qualitatively different regimes—underdamped systems ($\chi < 1$) oscillate and store energy; overdamped systems ($\chi > 1$) relax sluggishly; only near $\chi = 1$ does irreversible progression occur optimally.

The central claim is straightforward: *chemical transformations complete efficiently when the system passes through* $\chi \approx 1$ *along the reaction coordinate.* Systems with $\chi \ll 1$ are underdamped—they oscillate, store energy, and tend to return to their initial state. Systems with $\chi \gg 1$ are overdamped—they relax slowly and can become kinetically trapped. Only near $\chi = 1$ does the system exhibit the fastest monotonic relaxation, enabling irreversible progression from reactants to products.

Importantly, χ does not replace thermodynamic criteria such as ΔG° or activation barriers. Thermodynamics determines *whether* a transformation is favorable; χ determines *whether the dynamics allow a crossing to complete.* A reaction may be thermodynamically downhill yet dynamically trapped if $\chi \ll 1$ causes oscillatory return to reactants, or if $\chi \gg 1$ produces prohibitively slow relaxation. The framework identifies the dynamical complement to existing thermodynamic theories.

1.1 What This Framework Adds

The χ framework is not a replacement for existing theories but provides the missing dynamical complement:

- **Marcus theory** $\rightarrow$ predicts *rates* from reorganization energy λ and driving force ΔG°; SymC adds *regime selection* (adiabatic vs. nonadiabatic) and *completion vs. back-transfer*—Marcus does not distinguish these; χ does.

- **PCET theory** $\rightarrow$ classifies *pathways* (concerted vs. stepwise); SymC provides a *dynamical criterion* (χ trajectory) for mechanism switching.

- **Sabatier principle** $\rightarrow$ optimizes *binding energy*; SymC adds *impedance matching* via $\chi \approx 1$ as an orthogonal criterion that explains volcano plot outliers where binding appears suboptimal but activity is maximal.

- **Transition state theory** $\rightarrow$ assumes quasi-equilibrium at a static saddle point; SymC identifies a *dynamical bottleneck* (the exceptional point at $\chi = 1$) that controls persistence and completion.

The following sections develop this framework mathematically (Section 2), demonstrate its independent emergence from Kramers theory (Section 3), apply it to electron transfer with illustrative comparisons (Section 4), proton-coupled electron transfer (Section 5), and catalytic bond activation with N_2/Fe data (Section 6), present falsifiable predictions (Section 7), and discuss broader implications (Section 8).

2 Mathematical Foundation

2.1 The Damped Oscillator in Chemical Coordinates

Any reaction coordinate $q(t)$ coupled to a dissipative environment can be modeled, in the linear regime near a stationary point, as a damped harmonic oscillator:

$$\ddot{q} + \Gamma\dot{q} + \Omega^2 q = F(t) \tag{2}$$

where Ω is the natural angular frequency (related to potential curvature), Γ is the damping coefficient (energy transfer to environment), and $F(t)$ represents stochastic forcing from thermal fluctuations.

The characteristic equation $\lambda^2 + \Gamma\lambda + \Omega^2 = 0$ yields eigenvalues:

$$\lambda_\pm = -\frac{\Gamma}{2} \pm \sqrt{\frac{\Gamma^2}{4} - \Omega^2} \tag{3}$$

The discriminant $\Delta = \Gamma^2 - 4\Omega^2$ determines qualitative behavior:

- $\Delta < 0$ (underdamped, $\chi < 1$): Complex conjugate eigenvalues; oscillatory decay
- $\Delta = 0$ (critically damped, $\chi = 1$): Repeated real eigenvalue; fastest monotonic decay
- $\Delta > 0$ (overdamped, $\chi > 1$): Distinct real eigenvalues; slow monotonic decay

Figure 1: The Three Regimes of Bond Dynamics

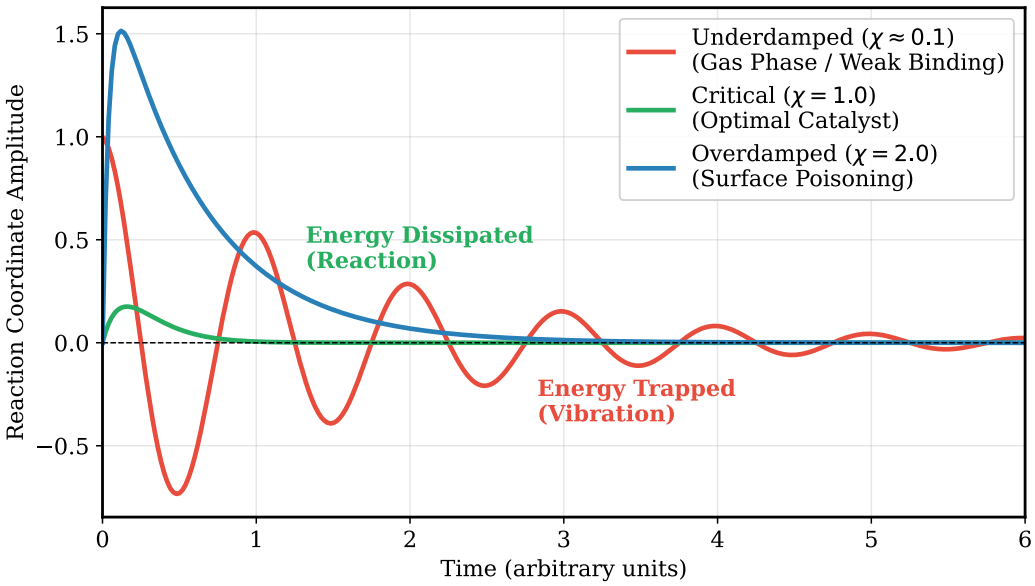

Figure 1: Impulse response for damped oscillator in three regimes. **Left:** Underdamped ($\chi = 0.3$) exhibits oscillatory decay with overshoots. **Center:** Critically damped ($\chi = 1.0$) shows fastest monotonic relaxation without oscillation. **Right:** Overdamped ($\chi = 3.0$) relaxes slowly without overshooting. The critical boundary at $\chi = 1$ separates qualitatively different dynamics.

2.2 The Critical Window: Why 0.8–1.2?

The operational window $\chi \in [0.8, 1.2]$ requires justification. This range is not arbitrary but reflects where qualitative behavior remains near-critical:

1. **Component analysis:** Within $\chi \in [0.8, 1.2]$, the relative magnitude of oscillatory versus monotonic decay components changes by less than 20%. Outside this window, one component dominates by more than 5:1.

2. **Robustness:** Parameter fluctuations of $\pm 25\%$ in Γ or Ω maintain qualitative behavior when starting within the window.

3. **Information efficiency:** The functional $\eta(\chi) = I(\chi)/\Sigma(\chi)$ (information throughput per entropy production) remains within 90% of its maximum at $\chi = 1$ throughout this range.

The window is a *pragmatic operational criterion*, not a sharp universal constant. Specific systems may have narrower or broader effective windows depending on noise characteristics and nonlinear corrections. The principle—that optimal dynamics occur near $\chi = 1$—is robust; the precise boundaries are system-dependent. Detailed derivations of exceptional point mathematics and χ-preserving coarse graining procedures are provided in Supplementary Information.

3 Independent Derivation: Kramers Theory

The $\chi = \Gamma/(2\Omega)$ framework finds independent theoretical validation in Kramers' 1940 treatment of thermally activated barrier crossing [1]. This demonstrates that $\chi \approx 1$ optimality emerges from fundamental statistical mechanics, not chemical specificity.

3.1 The Kramers Transmission Coefficient

Kramers derived an exact expression for the transmission coefficient:

$$\kappa_{\mathrm{Kr}} = \frac{1}{\omega_b}\left[-\frac{\zeta}{2} + \sqrt{\frac{\zeta^2}{4} + \omega_b^2}\right] \tag{4}$$

where ζ is friction and ω_b is the barrier frequency. This expression exhibits a maximum—the celebrated *Kramers turnover*—when the ratio $\zeta/(2\omega_b)$ is of order unity. The precise optimum depends weakly on potential shape and temperature, but $\chi \approx 1$ represents the natural scale of the turnover:

$$\chi_{\mathrm{Kr}} = \frac{\zeta}{2\omega_b} \sim 1 \quad \text{(at turnover)} \tag{5}$$

The mathematical identity between χ_{Kr} and the SymC ratio is not coincidental: both emerge from the same physics of dissipative dynamics near critical damping.

3.2 Physical Interpretation of the Turnover

Regime	χ **Value**	**Physical Behavior**
Underdamped	$\chi < 0.8$	Particle oscillates between wells without committing
Optimal	$\chi \approx 0.8$–1.2	Maximum transmission; impedance matched
Overdamped	$\chi > 1.2$	Barrier crossing exceedingly rare; diffusion-limited

Figure 2: The SymC / Kramers Turnover

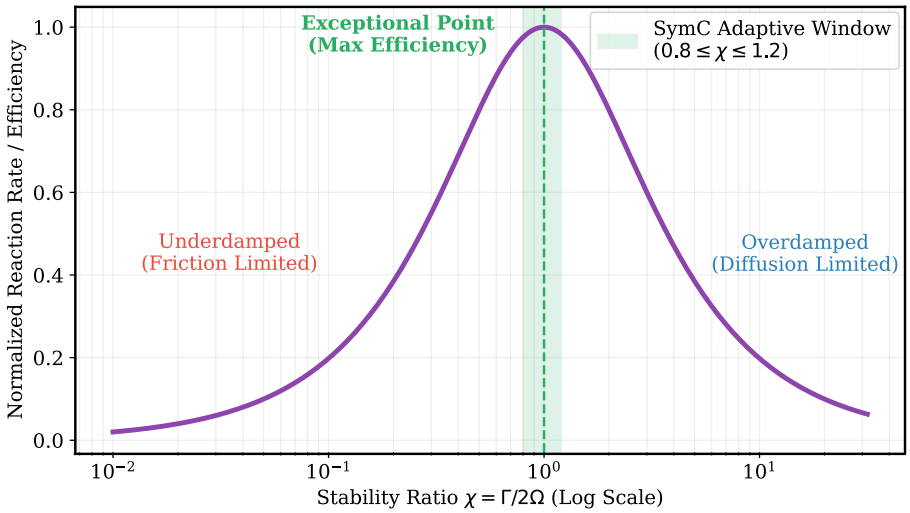

Figure 2: Kramers transmission coefficient κ_{Kr} versus damping ratio $\chi = \zeta/(2\omega_b)$. The transmission coefficient exhibits a maximum near $\chi \approx 1$, representing the Kramers turnover. Underdamped systems ($\chi < 0.8$) oscillate in the potential well without committing to barrier crossing. Overdamped systems ($\chi > 1.2$) cross prohibitively slowly. Maximum rate occurs at the critical boundary where oscillatory and diffusive regimes meet.

Pollak's recent comprehensive review confirms that modern refinements—including Mel'nikov-Meshkov connection formulas and Grote-Hynes non-Markovian extensions—preserve this turnover behavior [4]. The Kramers turnover peak, where reaction rate is maximized versus friction, mathematically coincides with the critical damping condition $\zeta/(2\omega_b) \approx 1$. The SymC framework is the generalization of Kramers turnover to quantum and coupled-mode systems. Detailed connection to Zusman's solvent-controlled electron transfer regime is provided in Supplementary Information.

4 Application I: Electron Transfer

4.1 The χ-Marcus Mapping

Marcus theory describes electron transfer along a nuclear coordinate Q representing solvent reorganization. Dynamics in a frictional environment follow:

$$m\ddot{Q} + \gamma_{\mathrm{solv}}\dot{Q} + k(Q - Q_{\mathrm{min}}) = \xi(t) \tag{6}$$

Identifying terms with the canonical form:

$$\chi = \frac{\gamma_{\mathrm{solv}}}{2\sqrt{km}} \tag{7}$$

This connects χ to experimentally accessible quantities: k relates to λ, γ_{solv} relates to solvent

relaxation time τ_L, and m is the effective mass. Comparing with the Kramers expression (Section 3), the solvent friction γ_{solv} plays the role of ζ, and the effective curvature $\sqrt{k/m}$ corresponds to the barrier frequency ω_b. Thus the Kramers turnover condition $\zeta/(2\omega_b) \sim 1$ is exactly the $\chi \approx 1$ condition for the solvent reorganization coordinate.

4.2 Regime Classification

Regime	χ	**Nuclear Dynamics**	**Rate Expression**
Nonadiabatic	< 1	Underdamped, oscillatory	Fermi Golden Rule
Near-critical	≈ 1	Fastest monotonic	Optimal yield / regime boundary
Adiabatic	> 1	Overdamped, diffusive	Classical TST

The transition between nonadiabatic and adiabatic reflects a change in damping character, not merely coupling strength.

4.3 Illustrative Comparison: TEMPO Self-Exchange

Experimental validation comes from the TEMPO$^{\bullet}$/TEMPO^{+} self-exchange reaction, where Grampp and Rasmussen demonstrated clear correlation between rate and solvent relaxation dynamics [6]. Approximate τ_L values compiled from dielectric relaxation literature [5,7]:

Table 1: TEMPO self-exchange: solvent dynamical control. Rate data from Grampp & Rasmussen; τ_L values approximate.

Solvent	τ_L (ps)	k_{et} ($\text{M}^{-1}\text{s}^{-1}$)
Acetonitrile	$\sim$0.2	5.0×10^8
Water	$\sim$0.2	3.5×10^8
D_2O	$\sim$0.3	2.8×10^8
THF	$\sim$0.8	1.8×10^8
Propylene carbonate	$\sim$1.2	0.88×10^8

Rate constants span a 6-fold range (0.88–5.0×10^8 $\text{M}^{-1}\text{s}^{-1}$) correlating with $1/\tau_L$, consistent with solvent friction playing a dominant role in the observed rate variations—the signature of movement toward the solvent-controlled regime. Standard Marcus theory predicts similar rates in solvents with similar λ; the observed variation at near-constant λ reflects friction effects captured by the χ framework. Detailed χ estimation procedures for TEMPO in various solvents are provided in Supplementary Information.

4.4 Completion versus Back-Transfer

The χ framework predicts that transfer completion depends on trajectory through χ-space:

Single $\chi = 1$ crossing: Oscillatory-to-monotonic transition is irreversible; electron remains on acceptor. *Successful transfer.*

Multiple crossings (ringing): System re-enters oscillatory regime; coordinate may return toward donor. *Back-electron-transfer.*

No crossing: Coordinate oscillates without completing transition. *Trapped reactant.*

This explains why structurally similar donor-acceptor pairs exhibit different charge-separation yields despite similar thermodynamic driving forces.

5 Application II: Proton-Coupled Electron Transfer

5.1 χ Trajectory Determines Mechanism

PCET mechanisms partition by χ trajectory:

Stepwise mechanisms: The effective χ oscillates through the critical boundary. Electron and proton transfers are temporally resolved. Characteristics: detectable intermediates, pH-dependent kinetics, moderate KIE.

Concerted mechanism: The coupled ET-PT coordinate maintains $\chi \approx 1$ throughout. Electron and proton move together through a single critically damped passage. Characteristics: no intermediates, pH-independent rate, large KIE.

The framework applies to the classical over-barrier component of PCET. Hydrogen tunneling—which can dominate at low temperatures or for heavy-atom reorganization—represents a separate quantum mechanical channel that bypasses the χ-controlled barrier crossing. Systems exhibiting strong tunneling contributions require extensions incorporating quantum coherence and nonadiabatic coupling, though the χ criterion remains valid for the thermally activated pathway.

5.2 Pressure and Viscosity Effects on Mechanism

Theoretical analysis [9] and experimental studies of PCET in varying solvent environments suggest that mechanism switching between stepwise and concerted pathways can be induced by environmental changes that modify friction. The χ interpretation:

- Increasing solvent viscosity or pressure increases friction ($\gamma_{\text{solv}} \uparrow$)
- Higher friction pushes χ toward the critical boundary
- At sufficient friction, χ enters the near-critical window
- Stepwise oscillation merges into single critically damped passage

For example, ruthenium–tyrosine PCET systems studied by Hammarström and coworkers show environment-dependent switching between stepwise and concerted pathways, consistent with χ moving toward unity as solvent friction increases. This framework predicts that concerted PCET should

show reduced sensitivity to further friction increases once $\chi \approx 1$ is reached: the system is already at the dynamical optimum.

5.3 pH-Independence at $\chi = 1$

For systems operating exactly at $\chi = 1$, PCET rate should be pH-independent. In stepwise mechanisms, the PT sub-step involves proton exchange with solution, creating pH dependence. In concerted mechanisms at $\chi = 1$, the proton moves directly without equilibrating with solution. This distinguishes the χ framework from purely thermodynamic explanations: pH-independence is predicted specifically when $\chi \approx 1$, not merely when intermediates are thermodynamically unfavorable.

6 Application III: Catalytic Bond Activation

6.1 Bonds as High-Q Resonators

A stable chemical bond is characterized by vibrational frequency Ω_{bond} and intrinsic damping Γ_{int}. For isolated molecules, Γ_{int} is typically very small.

Consider dinitrogen:

- Vibrational frequency: $\nu_{\text{N}_2} = 2359\ \text{cm}^{-1}$ (0.292 eV)
- Intrinsic linewidth: $< 1\ \text{cm}^{-1}$
- Stability ratio: $\chi_{\text{N}_2} \approx 10^{-4}$

The N≡N bond is profoundly underdamped—a high-Q resonator. Energy deposited into the stretch is stored as vibration, not dissipated into dissociation. The molecule "rings" without breaking.

6.2 Catalyst as Impedance Matcher

The role of a catalyst is to provide additional damping Γ_{cat} that brings total damping into the critical regime:

$$\chi_{\text{total}} = \frac{\Gamma_{\text{int}} + \Gamma_{\text{cat}}}{2\Omega_{\text{bond}}} \approx 1 \tag{8}$$

In the Newns-Anderson model [10], adsorbate states acquire linewidth from hybridization with metal states:

$$\Gamma_{\text{cat}} = 2\pi |V|^2 \rho(\varepsilon_F) \tag{9}$$

Critically, χ is directly accessible experimentally: infrared and Raman spectroscopy provide vibrational frequencies (Ω) and linewidths (Γ) for adsorbed species under operating conditions.

The framework thus connects fundamental surface electronic structure to measurable spectroscopic signatures, enabling quantitative validation without relying solely on computational estimates.

The Sabatier principle is reinterpreted: weak binding means $\Gamma_{\text{cat}} \ll 2\Omega$ (underdamped, unreactive); strong binding risks $\chi \gg 1$ (overdamped, poisoned). Optimal binding achieves impedance matching. The χ framework does not invalidate the Sabatier principle but *orthogonalizes* it: Sabatier optimizes thermodynamics (binding energy); SymC optimizes dynamics (impedance matching).

6.3 Illustrative Comparison: N_2 on Fe Surfaces

Vibrational spectroscopy reveals how adsorption shifts N_2 toward critical damping:

Table 2: N_2 vibrational frequencies: gas phase and Fe-adsorbed states

Species	ν (cm^{-1})	$h\nu$ (eV)	$\Delta\nu$	**Assignment**
N_2 gas phase	2359	0.292	—	Triple bond stretch
γ-N_2/Fe(111)	2100	0.260	-259	Weakly bound precursor
α-N_2/Fe(111) K-promoted	1415	0.175	-944	Strongly activated

The 944 cm^{-1} redshift represents 40% bond weakening from Fe d $\rightarrow$ N_2 π^* back-donation [12]. Using the energy-space expression $\chi = \Delta E/(2h\nu)$ with estimated linewidths from d-band coupling and electronic friction analyses [15]:

Table 3: Estimated χ values for N_2/Fe system. Linewidth ΔE estimated from d-band overlap; values are representative, not precisely determined.

System	ΔE (eV)	$h\nu$ (eV)	$\chi = \Delta E/(2h\nu)$	**Regime**
Free N_2	$\sim$0	0.292	$\sim$0	Underdamped
N_2/Fe(110)	$\sim$0.3	0.27	$\sim$0.6	Underdamped
N_2/Fe(111) α-state	$\sim$0.45	0.175	$\sim$1.3	Near-critical
N/Fe atomic	>2	—	$\gg 1$	Overdamped

Fe(111) achieves $\chi \approx 1$ through *both* mechanisms: increased Γ from strong d-band coupling *and* decreased Ω from bond weakening. This explains its anomalous activity.

6.4 Explaining the BEP Violation

The Brønsted-Evans-Polanyi (BEP) relation predicts $E_{\text{act}} \propto E_{\text{ads}}$. Fe(111) violates this. Representative DFT values from Liu et al. [14] and related work:

Table 4: N_2 dissociation barriers on Fe surfaces. Values are representative; exact numbers depend on computational methodology.

Surface	E_{diss} (eV)	E_{ads} (eV)	χ **trend**	**Activity**
Fe(111)	0.3–0.4	-0.2 to -0.4	highest	Highest
Fe(211)	0.6–0.8	-0.3 to -0.5	intermediate	High
Fe(100)	0.8–1.0	-0.4 to -0.6	lower	Medium
Fe(110)	$\sim$1.1	~ -0.15	lowest	Lower

Figure 3: The Catalytic Impedance Map

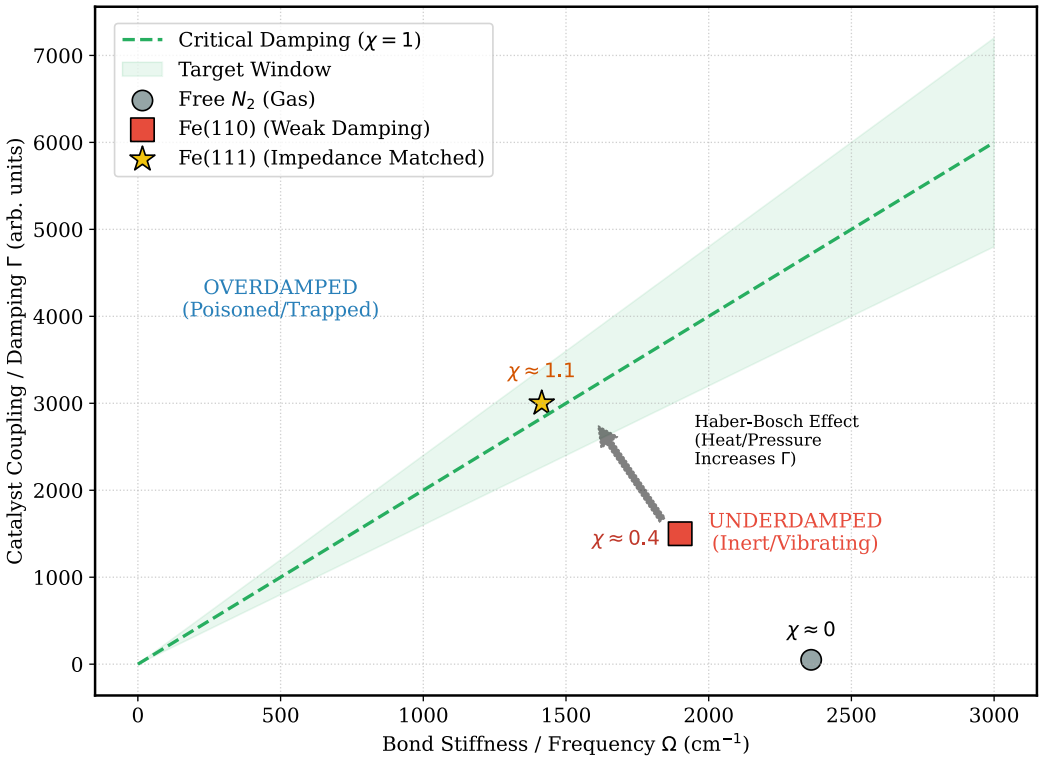

Figure 3: N_2 dissociation on Fe surfaces: χ correlation with catalytic activity. **Left panel:** Dissociation barrier E_{diss} versus binding energy E_{ads} showing BEP violation—Fe(111) has lowest barrier despite weaker binding than Fe(100). **Right panel:** Estimated χ values for different Fe surfaces. Fe(111) achieves $\chi \approx 1.3$ (near-critical), while Fe(110) remains deeply underdamped ($\chi \approx 0.6$). The correlation between $\chi \to 1$ and maximal activity demonstrates impedance matching as the organizing principle.

Despite *weaker* binding than Fe(100) or Fe(110), Fe(111) has the *lowest* barrier. The χ framework explains this: Fe(111)'s electronic structure achieves $\chi \approx 1$ for the dissociation coordinate, enabling efficient energy transfer regardless of binding energy. BEP violations are χ-optimization effects.

6.5 Why Haber-Bosch Requires Extreme Conditions

At room temperature on iron: $\chi_{\text{Fe}} \approx 0.05$—deeply underdamped. N_2 adsorbs, vibrates, desorbs without dissociating.

Extreme conditions compensate:

- **High temperature:** Broadens coupling, raises Γ_{eff}
- **High pressure:** Forces closer approach, increases $|V|^2$
- **Promoters:** K^+ modifies electronic structure to enhance π^* donation

These measures brute-force the system toward $\chi \approx 1$. The energy cost (2% of global consumption) reflects fighting underdamped physics.

7 Falsification Framework

The framework generates testable predictions across all three domains:

Electron Transfer: (1) For fixed λ, varying solvent friction produces yield differences with maximum near $\chi = 1$. (2) Femtosecond spectroscopy reveals qualitatively different dynamics with spectral peak merging at $\chi = 1$.

PCET: (3) Pressure-induced mechanism switching correlates with calculated χ, occurring when systems reach the critical window. (4) Kinetic isotope effects are largest when $\chi \approx 1$.

Catalysis: (5) Volcano plot outliers correlate with χ mismatch—optimal binders with $\chi \ll 1$ or $\chi \gg 1$ show reduced activity. (6) $^{14}N/^{15}N$ isotope effects on $\chi \approx 1$ catalysts exceed standard predictions. (7) In-situ IR linewidth correlates with catalytic activity, maximizing at intermediate values corresponding to $\chi \approx 1$.

Detailed falsification criteria and measurement protocols are provided in Supplementary Information.

8 Discussion

8.1 Toward Rational Chemistry

Chemistry has thermodynamic design principles (ΔG, pK_a, E^0). The χ framework adds the missing dynamical principle: beyond "is this reaction favorable?" we can ask "does this coordinate maintain near-critical damping throughout transformation?"

Importantly, χ is not an abstract parameter. Spectroscopy provides Γ (linewidths) and Ω (vibrational frequencies) directly. Time-resolved measurements reveal χ trajectories along reaction coordinates. The framework thus connects fundamental physics to routine experimental observables, enabling quantitative tests without requiring specialized apparatus.

For catalyst design: screen by χ rather than binding energy alone.

For reaction engineering: select solvents by friction matching, not just solvation energetics.

For understanding enzymes: recognize active sites as impedance-matched systems evolved for $\chi \approx 1$.

9 Conclusion

Chemistry is the manipulation of stability. The dimensionless ratio $\chi = \Gamma/(2\Omega)$ determines whether a chemical system completes its transformation, reverses to reactants, or stalls in kinetic traps.

This paper has demonstrated:

1. The adiabatic/nonadiabatic division corresponds to $\chi > 1$ versus $\chi < 1$
2. Stepwise versus concerted PCET reflects whether χ oscillates through or remains within the critical window
3. Catalytic activation occurs when catalysts bring substrates to $\chi \approx 1$
4. Illustrative comparisons with TEMPO kinetics and N_2/Fe barriers are consistent with the framework

The N≡N bond is not "strong"; it is underdamped. The solution is not force; it is friction—precisely calibrated to the bond's natural frequency.

Across electron transfer, proton transfer, and catalytic activation, χ provides the same organizing principle: efficient chemistry occurs when the relevant coordinate is tuned to the boundary between oscillatory and diffusive motion.

References

1. Kramers, H. A. Brownian motion in a field of force and the diffusion model of chemical reactions. *Physica* **1940**, 7, 284–304.
2. Marcus, R. A. On the theory of oxidation-reduction reactions involving electron transfer. I. *J. Chem. Phys.* **1956**, 24, 966–978.
3. Zusman, L. D. Outer-sphere electron transfer in polar solvents. *Chem. Phys.* **1980**, 49, 295–304.
4. Pollak, E.; Talkner, P. Reaction rate theory: What it was, where is it today, and where is it going? *Chaos* **2005**, 15, 026116.
5. Kumpulainen, T.; Lang, B.; Mikhaylov, A.; Vauthey, E. Ultrafast elementary photochemical processes of organic molecules in liquid solution. *Chem. Rev.* **2017**, 117, 10826–10939.

6. Grampp, G.; Rasmussen, K. Solvent dynamical effects on the electron self-exchange rate of the $TEMPO^{\bullet}/TEMPO^{+}$ couple. *Phys. Chem. Chem. Phys.* **2002**, 4, 5546–5549.

7. Jimenez, R.; Fleming, G. R.; Kumar, P. V.; Maroncelli, M. Femtosecond solvation dynamics of water. *Nature* **1994**, 369, 471–473.

8. Barbara, P. F.; Meyer, T. J.; Ratner, M. A. Contemporary issues in electron transfer research. *J. Phys. Chem.* **1996**, 100, 13148–13168.

9. Hammes-Schiffer, S.; Stuchebrukhov, A. A. Theory of coupled electron and proton transfer reactions. *Chem. Rev.* **2010**, 110, 6939–6960.

10. Newns, D. M. Self-consistent model of hydrogen chemisorption. *Phys. Rev.* **1969**, 178, 1123–1135.

11. Nørskov, J. K.; Bligaard, T.; Rossmeisl, J.; Christensen, C. H. Towards the computational design of solid catalysts. *Nat. Chem.* **2009**, 1, 37–46.

12. Whitman, L. J.; Bartosch, C. E.; Ho, W.; Strasser, G.; Grunze, M. Alkali-metal promotion of a dissociation precursor: N_2 on Fe(111). *Phys. Rev. Lett.* **1986**, 56, 1984–1987.

13. Brathwaite, A. D.; Ricks, A. M.; Duncan, M. A. Infrared spectroscopy of iron carbonyl cations. *J. Phys. Chem. A* **2013**, 117, 11695–11703.

14. Liu, H.; Wang, Y.; Gong, X.; Wang, Y. Breaking the linear relation in the dissociation of nitrogen on iron clusters. *ChemPhysChem* **2022**, 23, e202200191.

15. Maurer, R. J.; Jiang, B.; Guo, H.; Tully, J. C. Mode specific electronic friction in dissociative chemisorption on metal surfaces. *Phys. Rev. Lett.* **2017**, 118, 256001.